Effect of finite-rate chemistry and unequal Schmidt numbers on turbulent non-premixed flames modeled with single-step chemistry

By J. H. Chen[1], S. Mahalingam[2], I. K. Puri[3] AND L. Vervisch[4]

The interaction between a quasi-laminar flame and a turbulent flowfield is investigated through direct numerical simulations (DNS) of reacting flow in two- and three-dimensional domains. Effects due to finite-rate chemistry are studied using a single-step global reaction A (fuel) $+B$ (oxidizer) $\rightarrow P$ (product), and by varying a global Damköhler number, as a result of which the turbulence-chemistry interaction in the flame is found to generate a wide variety of conditions, ranging from near-equilibrium to near-extinction. Differential diffusion effects are studied by changing the Schmidt number of one reactive species to one-half. It is observed that laminar flamelet response is followed within the turbulent flowfield, except in regions where transient effects seem to dominate.

1. Introduction

Due to the presence of kinetically influenced source terms in the species and energy equations, modeling of turbulent reacting flows is a complex and arduous task (Williams, 1985; Borghi, 1988). Classical approaches to turbulent combustion have generally sought to decouple the chemical kinetics from the fluid dynamics, such as in models involving the laminar flamelet concept (Williams, 1985; Peters, 1986), or the probability density function (pdf) approach which usually involves the hypothesis that mixing is unaffected by reactive processes (Kollmann, 1990).

The use of direct numerical simulations in investigations involving non-premixed flames, for a variety of circumstances that include extinction, is intrinsically attractive, since data is simultaneously available for the species concentrations, temperature, and flow dynamics. From this data, the determination of relevant quantities, both scalars and vectors, such as mixture fraction, scalar dissipation rate, reaction rate, strain rate, flame curvature, and stretch is straightforward and corresponds to a single-time/multiple-point experimental measurement of the same. As has been demonstrated for premixed flames (see Trouvé, 1991, Poinsot *et al*, 1991), DNS results are expected to provide an insight into the flow processes as well as an

1 Combustion Research Facility, Sandia National Laboratories, Livermore, CA
2 Center for Combustion Research, University of Colorado, Boulder, CO
3 Department of Mechanical Engineering, University of Illinois, Chicago, IL
4 Center for Turbulence Research

aid in the development of appropriate models of flame phenomena associated with turbulent non–premixed flames.

In this study, the source terms due to chemistry in the governing equations are retained by simplifying the chemical kinetics to an overall global step. The rate of this global step is varied in order to investigate conditions that extend from strong (near equilibrium) chemistry to weak (near extinction) chemistry. Modeling chemistry in the form of a single–step global reaction has served as a strong tool in the analytical investigation of laminar reacting flows (cf. Williams, 1985) and is expected to retain that purpose in the investigation of turbulent non–premixed flames through direct numerical simulation. Through the global step, it is assumed that fuel and oxidizer, i.e., species A and B, meet in stoichiometric proportion to form a single product, namely P. The species A, B, and P are assumed to have equal diffusivities in one set of simulations; in another set, in order to investigate effects due to differential diffusion, A is assumed to diffuse two times faster than B and P.

2. Model problem

The model problem involves a quasi–laminar flame interacting with decaying homogeneous and isotropic turbulence in a "rectangle" (2–D) or "box" (3–D) containing fuel and oxidizer on either side. At an initial time, the reaction zone is laminar although it is surrounded by a specified turbulent flow field. As time progresses the flame becomes unsteady and assumes turbulent characteristics. Boundary conditions stipulated at the boundaries that lie latitudinally to the flame, i.e., across it, are periodic while those that lie longitudinally, i.e., parallel to the flame, are non-reflecting (Poinsot, Lele 1991). Therefore, depending on the scale of the problem, the simulated "rectangle" or "box" represents instantaneous measurements in a flowfield corresponding to similar flow conditions that are represented by equivalent values of the local Reynolds, Damköhler, and Schmidt numbers. For instance, in the present simulations the Reynolds number based on the Taylor length scale, Re_t, has an initial value of fifty, the Damköhler number, Da, is assigned several values ranging from slow to fast chemistry, and the Schmidt number, Sc, for a select reactive species is assumed to be either unity or one–half. Studies of hydrogen–argon jet flames (Dibble *et al.*, 1986; Magre & Dibble, 1988) indicate that the Reynolds number based on the velocity profile half–width increases from fifty to eighty along the jet axis. We recognize that this analogy is somewhat imprecise, since the velocity and length scales that are involved differ, but are hampered by the unavailability of simultaneously obtained data, the precise facet that makes direct numerical simulations attractive.

3. Methodology

A compressible direct simulation code developed by Trouvé (1991) is utilized in this investigation. The code is able to simulate a reacting flow, including effects due to variations in density and viscosity. Various aspects of the methodology that are specific to this study are described below.

3.1 Chemistry

The chemical reaction is represented by a single–step global mechanism, i.e.,

$$A \text{ (fuel)} + B \text{ (oxidizer)} \rightarrow P \text{ (product)} . \tag{1}$$

The reaction rate is in the familiar Arrhenius form, namely

$$\dot{w} = K\rho Y_A \rho Y_B \exp\left(-\frac{T_a}{T}\right), \tag{2}$$

which can be transformed such that (Williams, 1985),

$$\dot{w} = \mathbf{K}\rho Y_A \rho Y_B \exp\left(\frac{-\beta(1-\Theta)}{1-\alpha(1-\Theta)}\right). \tag{3}$$

In the above equations, the symbol Θ is a reduced temperature, such that $\Theta = (T - T_o)/(T_f - T_o)$, T_f is the adiabatic flame temperature and T_o the ambient temperature; T_a denotes the activation temperature; K is a pre–exponential factor; α and β respectively denote a temperature factor and the dimensionless activation energy; and $\mathbf{K} = K\exp(-\beta/\alpha)$. In the present study, databases have been generated for the case : $\beta = 8$, $\alpha = 0.8$; these values are close to the overall characteristics of methane air combustion.

3.2 Conservation equations

The equation of state is assumed to hold true in the flowfield, and without loss of generality, the fuel, oxidizer, and product are assumed to be of equal molecular weight. The dynamic viscosity μ is assumed to be a function of temperature, such that $\mu = \mu_o(T/T_o)^a$, the exponent a being assigned a value of 0.76. The thermal conductivity λ and mass diffusivities $\mathcal{D}_A$, $\mathcal{D}_B$ that appear below are related to the dynamic viscosity through the Prandtl and Schmidt numbers, the subscripts A and B corresponding to the relevant species. The value of the Prandtl number is unity in the present simulations.

In a Cartesian frame of reference, the conservation equations are of the form:

$$\frac{\partial \rho}{\partial t} + \frac{\partial \rho u_i}{\partial x_i} = 0 , \tag{4}$$

$$\frac{\partial \rho u_i}{\partial t} + \frac{\partial \rho u_i u_j}{\partial x_j} = -\frac{\partial p}{\partial x_i} + \frac{\partial \tau_{ij}}{\partial x_j} , \tag{5}$$

$$\frac{\partial \rho E}{\partial t} + \frac{\partial (\rho E + p)u_i}{\partial x_i} = \frac{\partial (u_j \tau_{ij})}{\partial x_i} + \frac{\partial}{\partial x_i}\left(\lambda \frac{\partial T}{\partial x_i}\right) + Q\dot{w} , \tag{6}$$

$$\frac{\partial \rho Y_A}{\partial t} + \frac{\partial \rho Y_A u_i}{\partial x_i} = \frac{\partial}{\partial x_i}\left(\rho \mathcal{D}_A \frac{\partial Y_A}{\partial x_i}\right) - \dot{w} . \tag{7}$$

$$\frac{\partial \rho Y_B}{\partial t} + \frac{\partial \rho Y_B u_i}{\partial x_i} = \frac{\partial}{\partial x_i}\left(\rho \mathcal{D}_B \frac{\partial Y_B}{\partial x_i}\right) - \dot{w} . \tag{8}$$

where

$$\rho E = \frac{1}{2}\rho \sum_{k=1}^{3} u_k^2 + \frac{p}{\gamma - 1} \tag{9}$$

and

$$\tau_{ij} = \mu\left(\frac{\partial u_i}{\partial x_j} + \frac{\partial u_j}{\partial x_i} - \frac{2}{3}\delta_{ij}\frac{\partial u_k}{\partial x_k}\right). \tag{10}$$

In the above equations, the symbol ρ denotes the mass density, E the total energy, p the pressure, and Q the heat release per unit mass of fuel. The remaining symbols are associated with the usual quantities. The specific heat ratio, γ, is assumed to have a value of 1.4. The equations are made dimensionless by a reference length, L_o, the speed of sound, and reference values for the fuel and oxidizer mass fractions. In the manner discussed above, the temperature is converted into an appropriate reduced temperature. The equations are solved using a high-order finite difference scheme (Lele, 1989).

3.3. Turbulence and flame parameters studied

Through interaction with the turbulence, the initial laminar flame is strained by the vorticity, and both reactants and product are convected by it. The heat release interacts with the flow field within and outside the high reaction rate zone through effects that are due to dilatation and through variations of viscosity and diffusivities with temperature. Databases were generated for two-and three-dimensional flames for several conditions.

The initial turbulent kinetic energy spectrum function is given by:

$$E(k) = C_0 \frac{u_0^2}{k_0}\left(\frac{k}{k_0}\right)^4 \exp\left[-2\left(\frac{k}{k_0}\right)^2\right], \tag{11}$$

where k is the wavenumber, k_0 is the wavenumber corresponding to the most energetic eddies, and u_0 is the rms velocity. A spatial filter is used to reduce the velocity fluctuations within the initial laminar flame, thereby allowing the flame to be distorted by the turbulence prior to undergoing extinction. The initial Taylor Reynolds number based on the cold fluid viscosity is fifty. The ratio of the initial reaction zone thickness, δ_{fl}, to the Kolmogorov scale is the order of ten.

The initial global Damköhler number defined as:

$$Da = \frac{l_t}{u_0}\left[\frac{1}{\delta_{fl}}\int_{\delta_{fl}} \dot{w} dx\right] \tag{12}$$

is a ratio of the eddy turnover time to a characteristic chemical reaction time based on the heat release. The databases have been investigated for a time equal to 1.6 eddy turnover times.

3.4. Initial conditions

Initially, fuel and oxidizer exist on either side of a domain separated by a laminar non–premixed flame. The initial turbulence spectrum and velocity field are specified in the domain, after which the governing equations are advanced in time. The initial distribution of reactant and product concentration in the laminar flame is obtained from a one–dimensional computation, the result of which is displayed in Figure 1(a). The velocity profile across the flame is presented in Figure 1(b). Note that velocity increases monotonically across the flame. Effects due to dilatation are apparent in the reaction zone which can be identified from the species concentration profiles of Figure 1(a). The initial laminar flame obeys the conservation equations, and the physical properties of this flame are well known. As a check, the growth of the laminar flame is investigated with respect to time. The thickness of the flame, δ_{fl}, is determined to grow in proportion to the square root of time, t, a result that is presented in Figure 1(c).

4. Results and discussion

In order to analyze various characteristics of the flame–turbulence interaction, we describe the reacting flowfield globally, as well as specifically, in terms of the flame topology. In addition, field statistics are obtained in a manner relevant to model construction and validation. At this juncture, additional descriptions are introduced, namely for the mixture fraction and the scalar dissipation. The mixture fraction, Z, is given in the form :

$$Z = \frac{1}{2}(1 + Y_A - Y_B) \tag{13}$$

The fuel and oxidizer vanish at the stoichiometric surface when fast chemistry prevails, such that at this location $Z = Z_{st} = 0.5$ in the simulations. The mixture fraction is a conserved scalar when each of the species involved in the reacting flow has equal mass diffusivities and is, obviously, not conserved when the Schmidt number of any one of the species is changed as is done in some of the simulations. However, in order to make global comparisons between differing situations involving a variety of length and time scales, investigators have generally found it instructive to examine the global description of non–premixed flames with respect to the mixture fraction, even for those cases when this quantity is not conserved.

The scalar dissipation rate, χ, is related to the gradient of the mixture fraction and is given as :

$$\chi = 2D|\nabla Z|^2 . \tag{14}$$

4.1. Global description

Postprocessing of the databases indicates that a global description of the two–and three–dimensional flames is essentially similar. Therefore, for sake of brevity, only the two-dimensional results are discussed in this subsection. Flames corresponding to high enough Damköhler numbers, i.e., greater than of order unity, burn vigorously, such that an equilibrium based description of the chemistry is adequate,

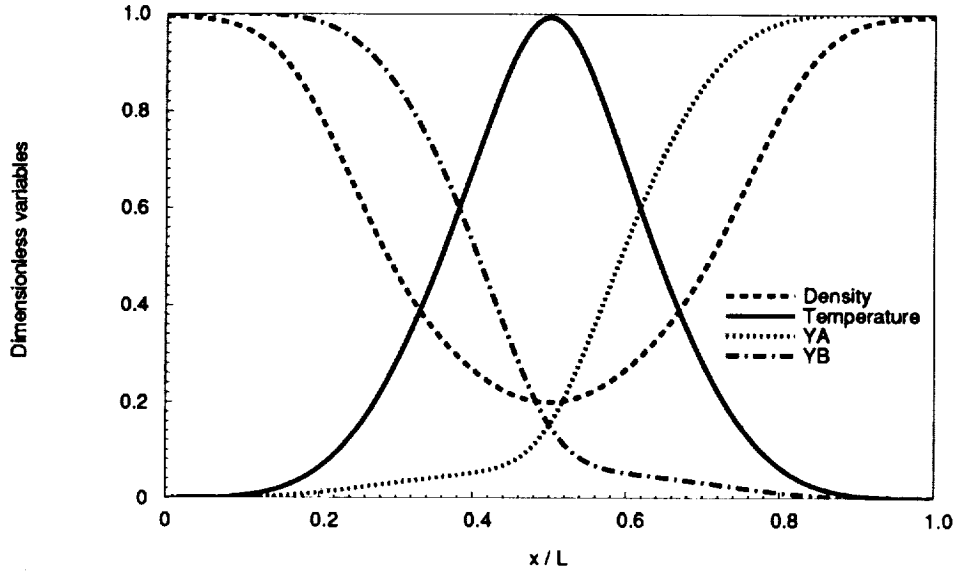

FIGURE 1(A). Species concentration profiles across the flame for a representative condition (1–D simulation, $Da = 1$).

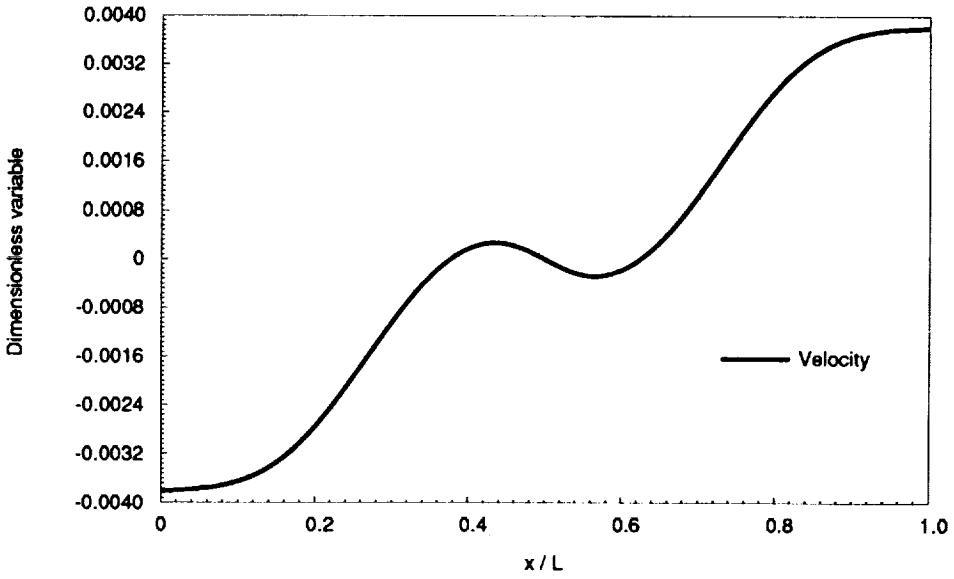

FIGURE 1(B). Velocity profile across the flame for a representative condition (1–D simulation, $Da = 1$).

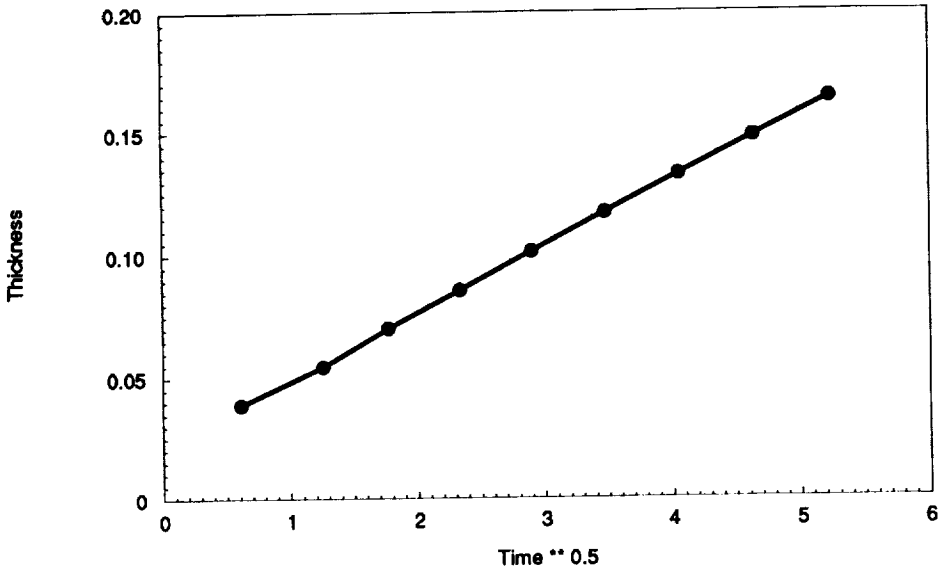

FIGURE 1(C). The growth of the laminar flame thickness with time for a representative condition (1–D simulation, $Da = 1$).

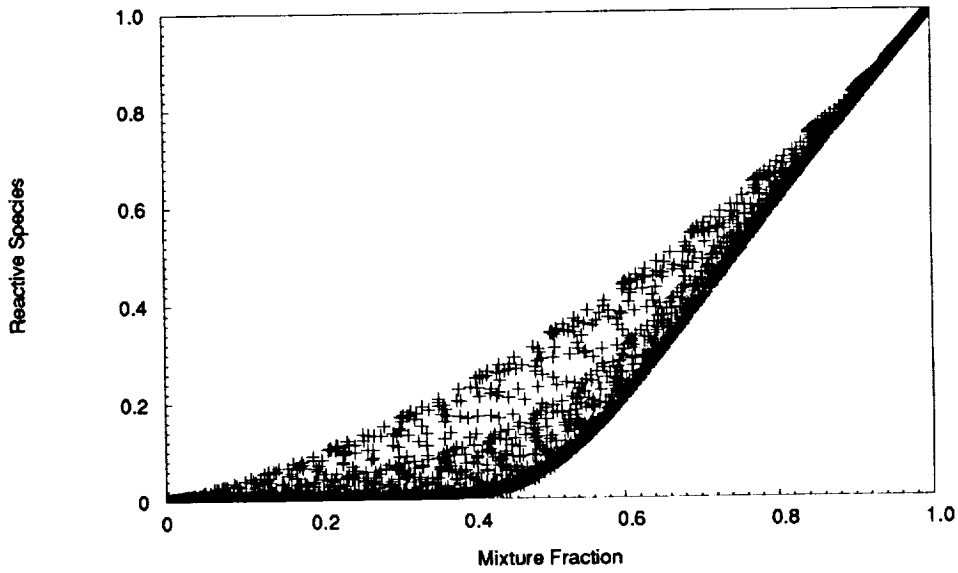

FIGURE 2(A). Distribution of the reactive species A (fuel) mass concentration with respect to the mixture fraction Z (2-D simulation, $Da = 1$).

whereas flames established at Da of $O(1)$ are close to extinction at conditions far from chemical equilibrium.

In Figure 2(a), we present the variation of the reactive species A (fuel) mass fraction with respect to the mixture fraction. The lower bound on the species concentration profile corresponds to those locations in the flame that experience "full" burning and the upper bound to those locations that are influenced by extinction and, hence, close to undergoing only mixing. The species distribution that lies between these two limits is due to turbulence–induced mixing, influencing both the fully burning and extinguished locations, and is, therefore, a transient response. We note that in the equilibrium (or fast–chemistry) limit, the reactive species would reach a negligible concentration at $Z = Z_{st}$, whereas in Figure 2, this location is shifted to the reactant B side, i.e., $Z \approx 0.39$, due to finite–rate chemistry effects.

The dissipation rate of the reactive species, χ_A, described in the form:

$$\chi_A = 2D| \nabla Y_A |^2 , \tag{15}$$

is a quantity that represents the magnitude of the gradient of A. This dissipation rate is presented in Figure 2(b). Two regions are immediately evident, corresponding to the results of Figure 2(a), related to pure mixing (frozen flow) and fully burning situations. In the fully burning case, the dissipation rate is negligible for $Z < 0.39$ (Figure 2(c)), whereas for the situation corresponding to extinction (frozen flow), a finite bound appears in the Figure 2(b). Clearly, penetration of the species A (fuel) has taken place in the oxidizer side, thereby creating, at the very least, a partially premixed situation. Whether and under what conditions this premixing causes local re–ignition will be the focus of a subsequent study.

The global temperature profile of the $Da = O(1)$ flames is similarly distributed between the limits corresponding to fully burning and pure mixing situations. For flames corresponding to $Da > O(1)$, the maximum value of the reaction rate invariably occurs at the location of the peak temperature. However, as is clear from Figure 3, this situation is altered for the $Da = O(1)$ flames. We recall that the first–order reaction rate (cf. Equation (1)) simultaneously depends on the local fuel and oxidizer mass fractions and the local temperature. Due to turbulence–induced convection of species and local extinction, which causes penetration and premixing of the reactive species, a high reaction rate can exist at lower temperature locations where there is sufficient fuel and oxidizer concentration to sustain the chemical reaction. Therefore, in the presence of extinction, high values of the local instantaneous reaction rate are distributed over a range of temperatures below the peak temperature that is found in the flame. For cases corresponding to $Da = O(1)$, the smearing of the reaction rate in the domain is caused by higher levels of local vorticity.

Flames established at a low ($O(1)$) Damköhler number, i.e., those experiencing local extinction, also possess thicker reaction zones in both physical and mixture fraction space than those corresponding to higher Da values. In Figure 4(a), we present the reaction rate profile for a flame with Da of $O(1)$. The effect of extinction is apparent in the results presented in this figure since, at the stoichiometric location,

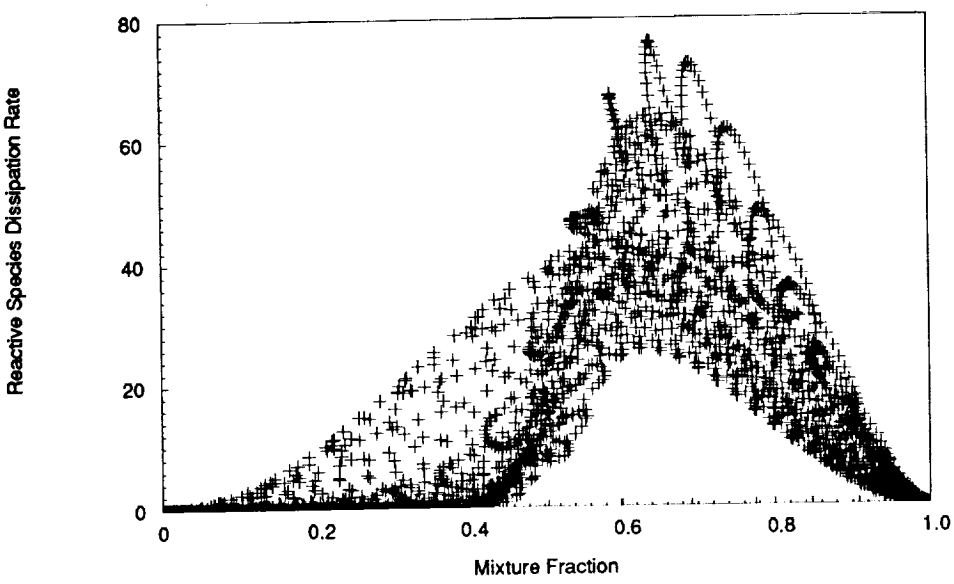

FIGURE 2(B). Distribution of the reactive species A (fuel) dissipation rate with respect to the mixture fraction Z (2-D simulation, $Da = 1$).

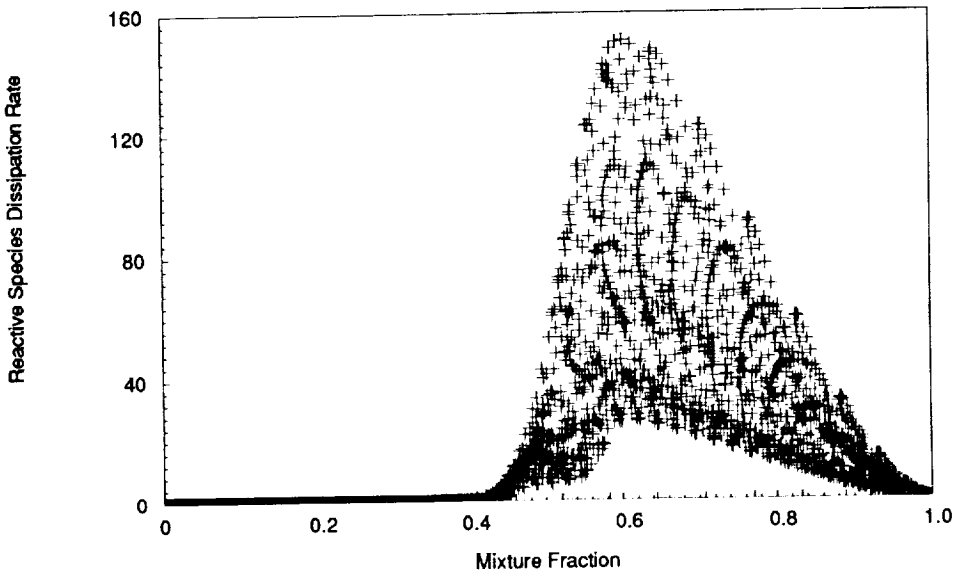

FIGURE 2(C). Distribution of the reactive species A (fuel) dissipation rate with respect to the mixture fraction Z (2-D simulation, $Da = 10$).

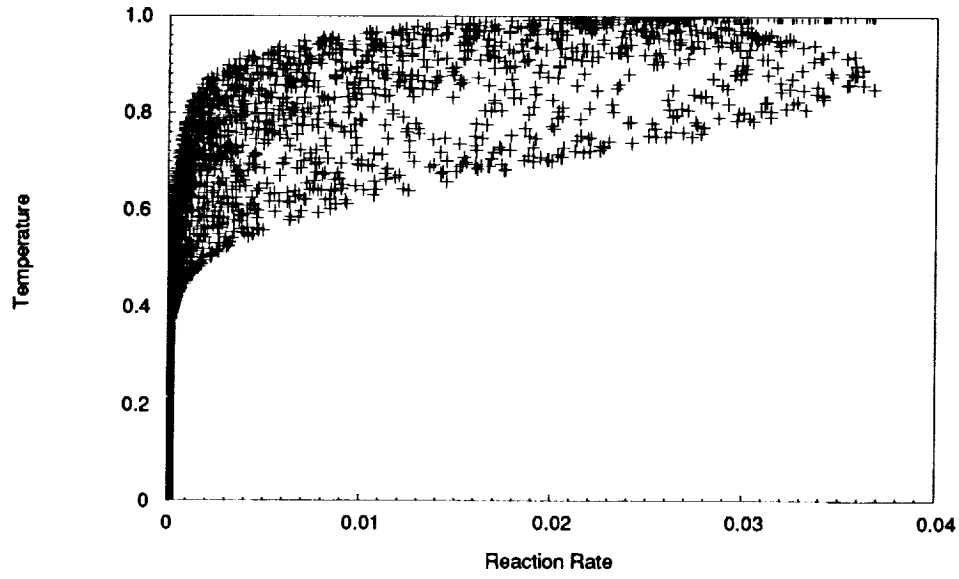

FIGURE 3. Distribution of the reaction rate $\dot{w}$ with respect to the reduced temperature (2-D simulation, $Da = 1$).

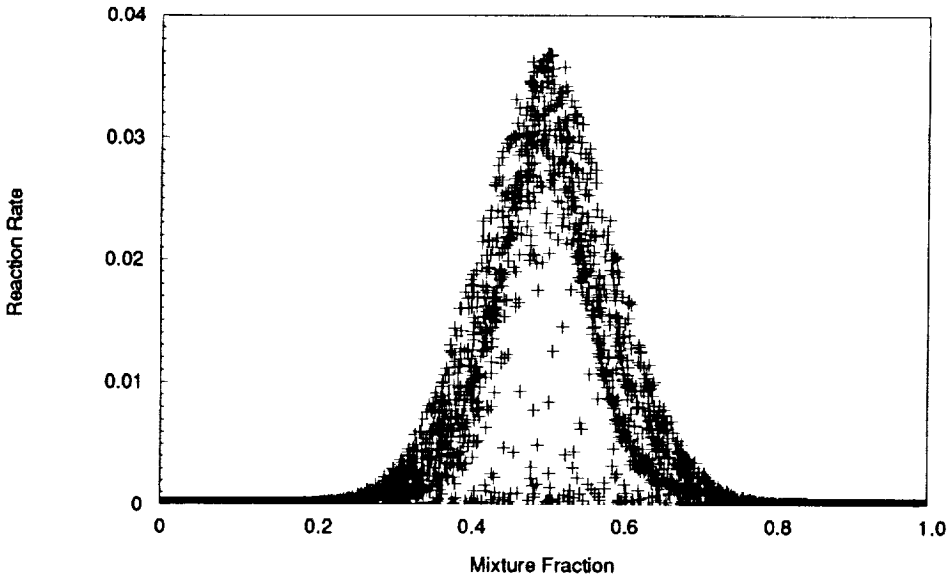

FIGURE 4(A). Distribution of the reaction rate $\dot{w}$ with respect to the mixture fraction Z (2-D simulation, $Da = 1$).

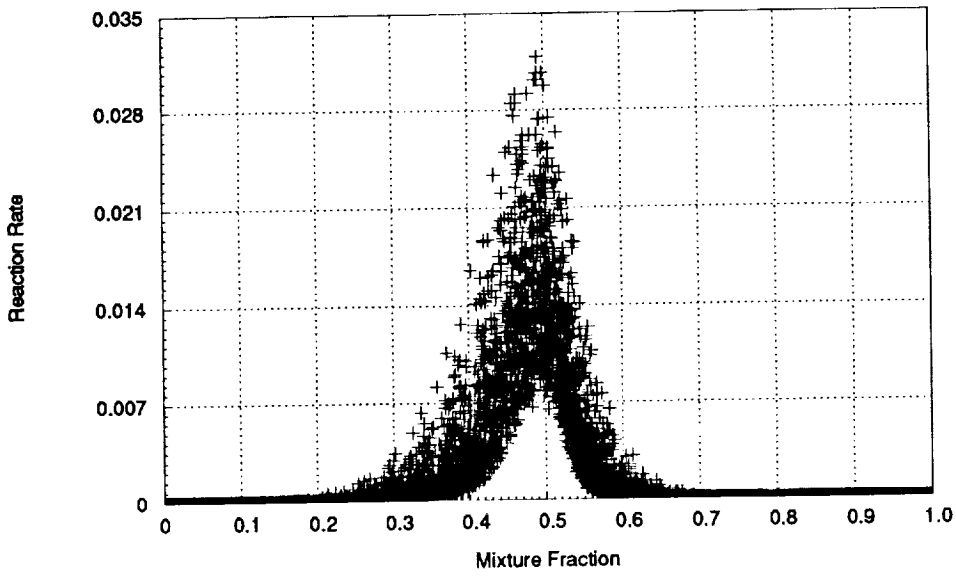

FIGURE 4(B). Distribution of the reaction rate $\dot{w}$ with respect to the mixture fraction Z (3-D simulation, $Da = 2.5$, $Sc_A = 0.5$).

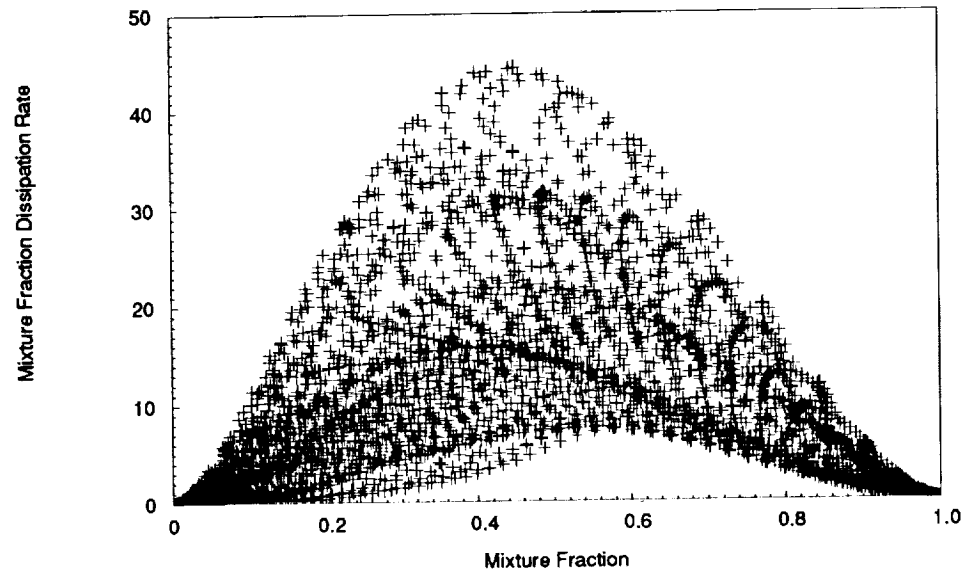

FIGURE 5(A). Distribution of the scalar dissipation rate, χ, with respect to the mixture fraction Z (2-D simulation, $Da = 1$).

C-5

there is both high and negligible reaction rate. Though the reaction rate reaches a maximum at the stoichiometric surface, Z_{st}, the reaction zone falls in a broad band around that location, spanning $Z \approx 0.3 - 0.7$. In contrast, the reaction zone corresponding to $Da = 10$, results for which are not displayed for sake of brevity, is thinner in both physical and Z– space (spanning $Z \approx 0.42 - 0.58$), with no evidence of local extinction, as is to be expected.

When the Schmidt number of the reactive species A (fuel) is decreased to a value of 0.5, the location of the peak reaction rate moves towards the "B–side" of the reaction zone since species A (fuel) diffuses faster than species B. Results for this situation are presented in Figure 4(b). We note that, for this case, the reaction zone is skewed and is broader on the "B–side". This is to be expected since reactant A, upon leakage through the reaction zone, will penetrate farther into for $Sc_B > Sc_A$. Conversely, the reaction zone on the "A–side" is thinner due to the inability of the species B to diffuse farther into A, after leaking through the reaction zone. The leakage of either reactant through the surface locating the maximum reaction rate is due to effects attributable to finite–rate chemistry. We note that when the Schmidt number of either reactant is different from unity, the mixture fraction is no longer a conserved scalar.

In accord with laminar flamelet theory, the scalar dissipation rate increases with the reaction rate and is somewhat symmetrically distributed about the stoichiometric surface. Results for χ are presented in Figure 5(a). The peak scalar dissipation rate in Figure 5(a) occurs on the oxidizer side, a phenomenon attributable to the slightly larger vorticity on that side (specified as part of the initial conditions) that causes more mixing and consequently larger gradients on that side. The χ profile lies within an envelope that appears to mark the response of a typical laminar–like flamelet. For instance, the inverse of the scalar dissipation rate after being appropriately normalized is indicative of a local Damköhler number (Peters, 1986). The instantaneous peak reaction rate associated with a laminar flamelet increases monotonically as this quantity is decreased, until abrupt extinction occurs (Williams, 1985). However, the classical hypothesis used in non-premixed flamelet modeling (Peters, 1986, Warnartz and Rogg, 1986) that Z and χ are uncorrelated, appears to be invalid, when the combustion occurs in the flamelet regime.

In Figure 5(b), we present the effect of Schmidt number on the scalar dissipation rate. The scalar dissipation rate is skewed away from the species that has a higher diffusivity. The higher diffusivity of species A smooths its spatial gradients and, as discussed above, simultaneously moves the reaction zone into the "B–side". The results of Figure 5(b) suggest a means to lower the local value of the instantaneous scalar dissipation rate by systematically involving differential diffusion effects. This has been identified as a topic of further investigation by this group.

4.2. Flame topology

The reaction zone is observed to undergo local extinction as the Damköhler number is reduced due to an increase in the local scalar dissipation rate or due to vorticity-induced strain. The flame surface becomes interrupted, as is apparent

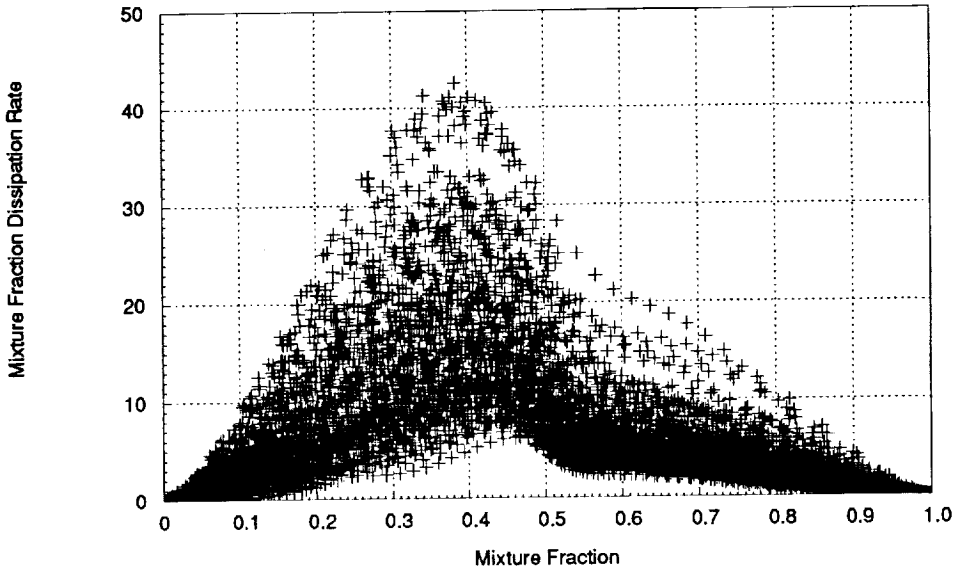

FIGURE 5(B). Distribution of the scalar dissipation rate χ with respect to the mixture fraction Z (3–D simulation, $Da = 2.5$, $Sc_A = 0.5$).

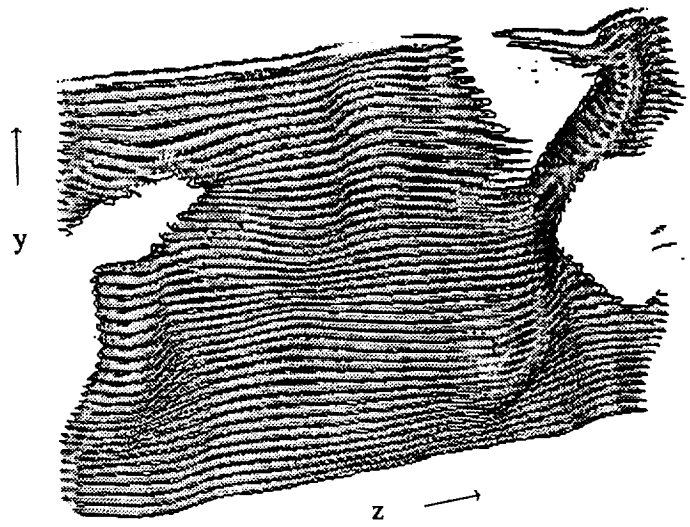

FIGURE 6. Distribution of the maximum reaction rate $\dot{w}$ in the turbulent flowfield (Y-Z plane, 3–D simulation, $Da = 1$).

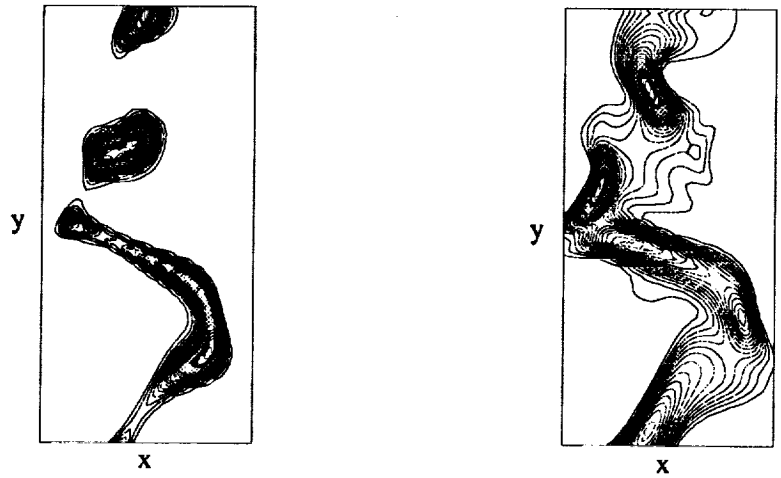

FIGURE 7(A) AND 7(B). On the left, distribution of the reaction rate; on the right, distribution of the scalar dissipation rate, at a specified z–location in the turbulent flowfield (3–D simulation, $Da = 1$)

from Figure 6. In this flame, "holes" occur where frozen flow, i.e., pure mixing, exists. In accord with laminar flamelet theory, the extinguished locations correspond to a high rate of the instantaneous scalar dissipation rate. This situation is clear in Figures 7(a) and 7(b), in which a flame is cut in the z–direction (corresponding to Figure 6) at a specified location and contours of the reaction and scalar dissipation rates are presented.

Extinction may also occur due to "flame–shortening" effects. This occurs when the product is not convected away at a rapid enough rate such that the reactive species are not present in a high enough concentration to sustain the chemical reaction. While we have observed the effect of flame–shortening in the two-dimensional databases, these effects are absent in the three-dimensional simulations, indicating the importance of including convection in a direction normal to (i.e. across) the reaction zone.

The flame presented in Figure 6 includes locations that are fully–burning and those that are close to extinction. We locate the stoichiometric surface and assume this to be the location of the peak reaction zone for the case corresponding to equal Schmidt numbers for all of the species (cf. Figure 4(a)). At this location, the scalar dissipation rate and the tangential strain rate are found to be well correlated as is apparent from Figure 8. Therefore, vorticity effects imply increasing tangential strain but also increased mixing and, consequently, larger gradients and dissipation rates. The extinguished locations in the flame presented in Figure 6 are a consequence of high local tangential strain rates.

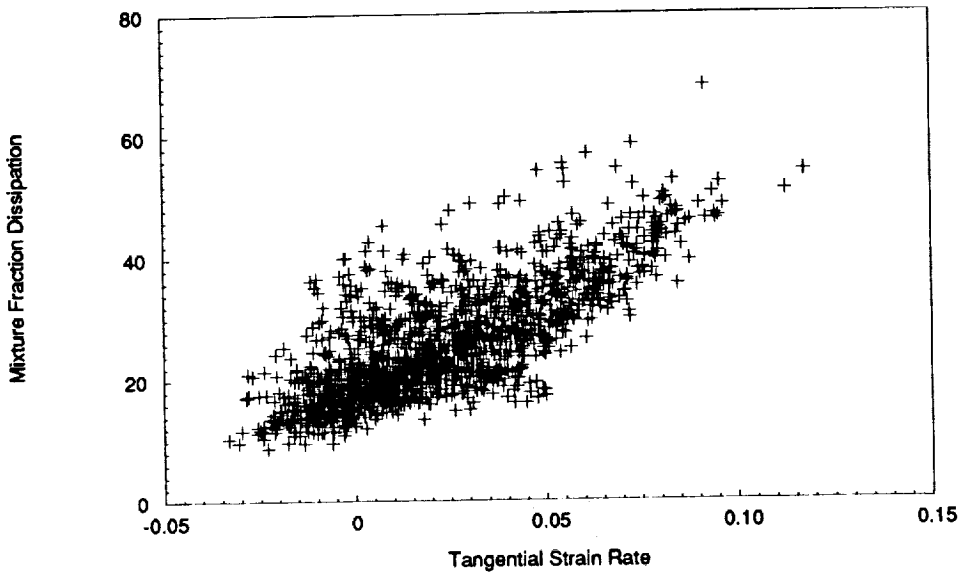

FIGURE 8. Correlation of the rate of strain tangential to the flame surface with the scalar dissipation rate, χ, along the flame surface (3–D simulation, $Da = 1$).

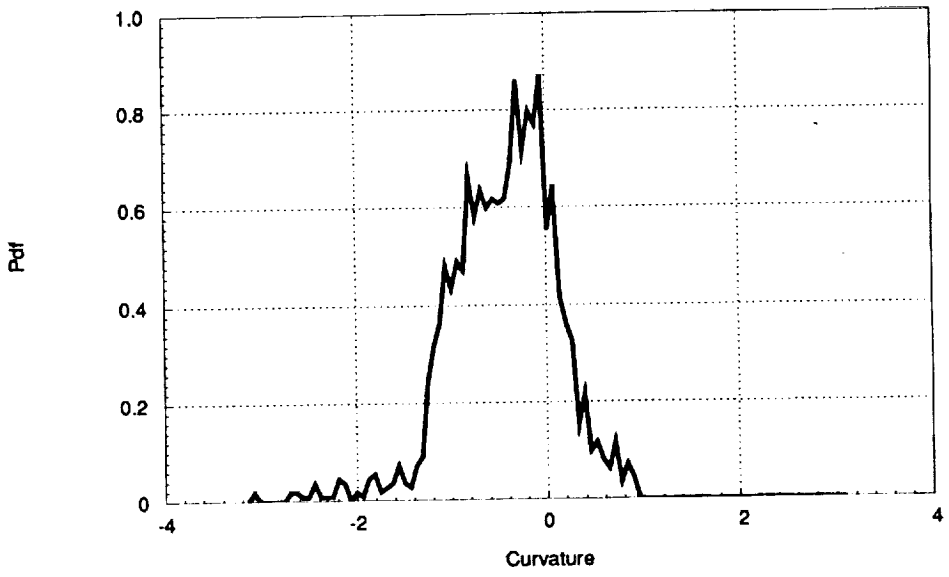

FIGURE 9. Probability density function of the curvature along the flame surface (3–D simulation, $Da = 2.5$, $Sc_A = 0.5$).

If the Schmidt number of all of the species is assigned a value of unity, the curvature of the three-dimensional flame is found to be symmetric, i.e, the stoichiometric surface exhibits both positive and negative curvature in an arbitrary reference frame. However, when the Schmidt number of the species A is changed to one-half, the probability of negative curvature along the stoichiometric surface increases. This result is presented in Figure 9. Negative curvature in this instance corresponds to flames that are curved into the B side. This observation is correlated with the figure 4(b), where the reaction zone is found to be broader on the B side.

A quantity of importance in mixing theories is the correlation coefficient between strain rate and scalar dissipation rate defined as:

$$\sigma = \frac{\langle \nabla Z \cdot e \cdot \nabla Z \rangle}{\langle e : e \rangle^{\frac{1}{2}} \langle \nabla Z \cdot \nabla Z \rangle},$$

where e is the rate of strain tensor. Gibson's (1968) theory for constant density flows predicts a value of -0.5 independent of Prandtl number (in this study, the Schmidt number is the appropriate quantity). Kerr (1985), Leonard, and Hill (1991) and Nomura and Elghobashi (1992) report values of this quantity in the range -0.4 to -0.5. Our simulations give a value of -0.6 when evaluated at the flame surface for $Da = 1$. The larger correlation is likely to be a result of dilatation associated with heat release in our computations. In Figure 10, the pdf of the magnitude of the cosine of the angle between the mixture fraction gradient and the principal strain rate directions at the flame surface is plotted. It is clear that the most probable alignment (Gamma) is one in which the scalar gradient is aligned with the most compressive strain rate direction. This picture is consistent with the computed correlation coefficient.

4.3. Field Structure

In order to compare the field structure of the simulated flames with that of laminar flamelets, we locate the stoichiometric surface and postprocess the data in order to interpolate the maximum reaction rate normal to this surface. The value of the peak reaction rate so obtained is presented with respect to the inverse of the scalar dissipation rate in Figure 11; the plotted values are made nondimensional using the reference values of the initial laminar flame. It is apparent that, for a given value of the maximum reaction rate, there exists a maximum value of the scalar dissipation rate (or a minimum value of $1/(\chi/\chi_{lam})$. Chemical reaction at that rate is not sustained if the corresponding maximum scalar dissipation rate is exceeded, and must increase. This dynamic situation continues until a critical value of the scalar dissipation rate is reached at which extinction occurs. The lower bound on that curve is a trace corresponding to the response of a typical laminar flamelet. However, as is obvious from Figure 11, the reaction rate–scalar dissipation response in the 3–D turbulent flame need not follow the typical laminar flamelet trace, thereby indicating circumstances under which the classical flamelet approach is inadequate.

The flamelet approach assumes that the length scales involved with the strain rate are much smaller than the small scales in the turbulent flow such that the

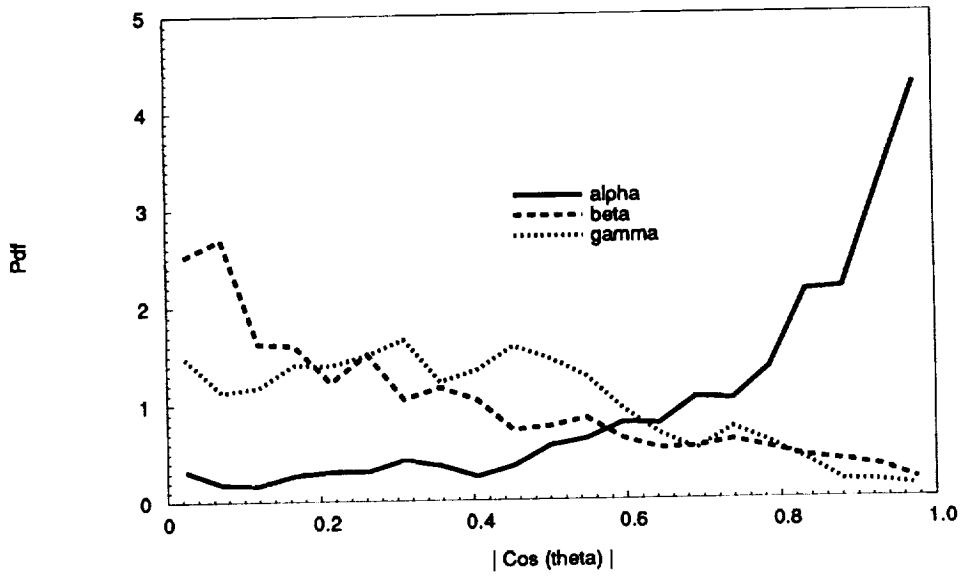

FIGURE 10. Pdf of the magnitude of the cosine of the angle between the scalar gradient and the principal strain directions (3–D simulation, $Da = 1$).

flame is strained by vorticity and convection in the outer flow. This circumstance holds true for the present simulations, in which it is apparent that vorticity does not penetrate the flame except at locations where extinction is observed. A contour map of the vorticity field is presented in Figure 12. In the high temperature region (where the reaction zone is located), the dynamic viscosity increases, which has the effect of locally damping the turbulence. If turbulence levels are high enough and the vorticity is not sufficiently decreased, extinction occurs (cf. Figure 7(a),(b) and 8). We speculate that deviation from the bounds indicated by laminar flamelet theory is due to a transient response involving finite rate chemistry, i.e., the peak value of the reaction rate lags changes to the local instantaneous scalar dissipation rate. The reason for this lag is due to the reaction rate being influenced not only by the local temperature but also by the local fuel and oxidizer mass fractions. The influence of extinction on the distribution of the reactive species is clear from Figures 2(a)–2(c). The effect of turbulence on the flame appears to be such that enhanced mixing convects more fuel (or oxidizer) to the reaction zone than in a purely diffusive situation or one corresponding to a typical laminar flamelet, thereby enhancing the local instantaneous reaction rate. The local temperature does not fall dramatically since the reactive species that is convected to the reaction zone comes from locations that are already hot (or at least warm). In Figure 13, the reactive species mass concentration at the reaction zone is presented for the case corresponding to Figure 11. The lower bound in this distribution is to be interpreted as that corresponding to the response of a laminar flamelet. It is obvious that higher

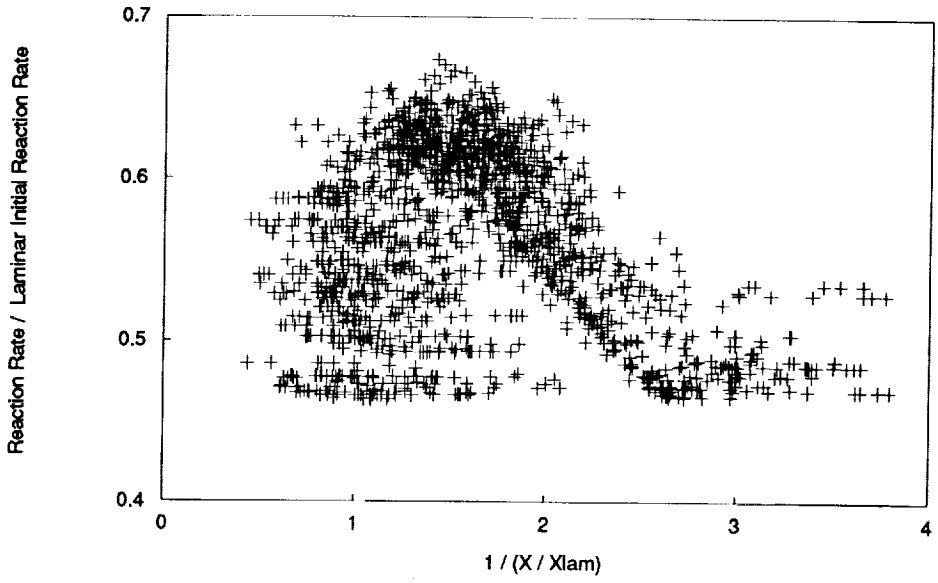

FIGURE 11. Distribution of the maximum reaction rate $\dot{w}$ mass concentration with respect to the inverse scalar dissipation rate $1/(\chi/\chi_{lam})$ (3–D simulation, $Da = 1$).

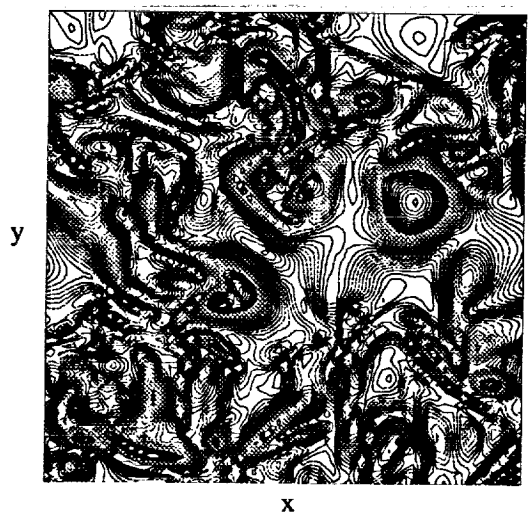

FIGURE 12. Distribution of the vorticity field in the turbulent flame (X-Y plane, 3–D simulation, $Da = 1$).

concentrations of reactive species are to be found than is proposed by flamelet theory. A systematic study of the seemingly transient effect induced by turbulent mixing has been identified as another topic of further investigation by this group.

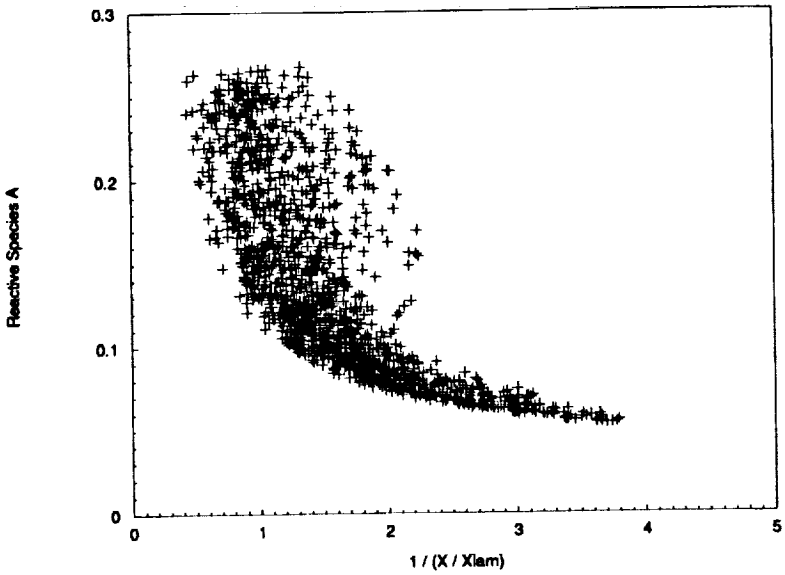

FIGURE 13. Distribution of the reactive species A mass concentration with respect to the inverse scalar dissipation rate $1/(\chi/\chi_{lam})$ (3–D simulation, $Da = 1$).

5. Conclusions and perspectives

Direct numerical simulations databases obtained using a compressible, variable property code have been investigated in order to study turbulent non–premixed flames established in two– and three–dimensional configurations. The flame is assumed to react fuel and oxidizer to form product through a global single–step reaction. A laminar flame is established at an initial time after which it is allowed to interact with a turbulent flowfield. From the databases that were thus created, the global description, flame topology, and field statistics are computed. The effects due to unequal species diffusivities is examined by changing the Schmidt number of one reactant.

The flames are found to extinguish when the scalar dissipation rate in the reaction zone exceeds a critical value. This rate, in turn, is well correlated with the tangential strain rate experienced by the flame. Flames that experience local extinction along the flame surface are found to exhibit global characteristics that are intermediate between those pertaining to frozen flow and fully burning situations. The reaction zones of such flames are thicker in both physical and mixture fraction space. It is determined that the scalar dissipation rate profile can be skewed with respect to the stoichiometric surface by effects stemming from unequal vorticity on the two sides

of the flame and, also, due to effects of unequal diffusivity. Differential diffusion also skews the curvature of the flame surface such that the flames are curved into the species that diffuses at a slower rate.

The response of the quasi-laminar flame is bounded by the characteristics typical of a laminar flamelet although significant deviation from this behavior is also observed. In particular, convection of reactants into the reaction zone suggests that the reaction rate may lag the change in scalar dissipation rate (or tangential strain rate) at the stoichiometric surface.

Several topics which require further investigation have been identified during this study. These include a study of the effects due to differential diffusion, the role of reignition in locally extinguished flames, and the deviation of the behavior of quasi–laminar flames from a flamelet–like behavior due to transient turbulence–related effects.

Acknowledgements

The authors have benefited from discussions with the other members of the combustion group during the 1992 CTR summer program, in particular with Dr. Arnaud Trouvé and Dr. Thierry Poinsot. We also thank Prof. Forman Williams and Prof. Stephen Pope for their helpful comments and suggestions. J. H. Chen has been supported for this work by the Department of Energy's Office of Basic Energy Sciences, Division of Chemical Sciences.

REFERENCES

BORGHI, R. 1988 Turbulent combustion modeling. *Prog. Energy Combust. Sci.* **14,** 245–292.

DIBBLE, R. W., SCHEFER, R. W., CHEN, J.-Y., HARTMANN, V. KOLLMAN, W. 1986 Velocity and density measurements in a turbulent nonpremixed flame with comparison to numerical model predictions. *Paper WSS/CI 86-65, Western States Section of the Combustion Institute Spring Meeting, Banff, Canada.*

GIBSON, C. H. 1968 Fine structure of scalar fields mixed by turbulence: I. Zero gradient points and minimal gradient surfaces. *Phys. Fluids.* **11,** 2305

KERR, R. M. 1985 Higher-order derivative correlations and alignment of small-scale structures in isotropic numerical turbulence. *J. Fluid Mech.* **153,** 31

KOLLMAN, W. 1990 The PDF approach to turbulent flow. *Theoret. Comput. Fluid Dynamics.* **1,** 249-285

LELE, S. 1989 Direct numerical simulation of compressible free shear flows. *27th Aerospace Sciences Meeting, AIAA 89-0374*

LEONARD A. D., HILL, J. C. 1988 Direct numerical simulation of a homogeneous turbulence reacting flow. *AIAA Paper No. AIAA-88-3624*

MAGRE, P., DIBBLE, R. W. 1988 Finite chemical kinetic effects in a subsonic turbulent hydrogen flame. *Combust. Flame.* **73,** 195–206.

NOMURA K. K., ELGHOBASHI 1992 Mixing characteristics of an inhomogeneous scalar in isotropic and homogeneous sheared turbulence. *Phys. Fluids.* **A4 (3),** March

PETERS, N. 1986 Laminar flamelet concepts in turbulent combustion. *Twenty-First Symposium (International) on Combustion.* 1231–1250. The Combustion Institute.

POINSOT T., VEYNANTE D., CANDEL S. 1991 Quenching processes and premixed turbulent combustion diagrams. *J. Fluid Mech.* **228,** 561–606

POINSOT, T., LELE, S. 1991 Boundary conditions for direct simulations of compressible viscous flows. *J. Comput. Phys.* **101,** No 1, July 92

TROUVE, A. 1991 Simulation of flame-turbulence interaction in premixed combustion. *Annual Research Briefs 1991.* CTR, Stanford U./NASA Ames.

WARNARTZ, J., ROGG, B. 1986 Turbulent non premixed combustion in partially premixed flamelets detailed chemistry. *Twenty-First Symposium (International) on Combustion.* 1533-1541. The Combustion Institute.

WILLIAMS, F. A. 1985 Combustion Theory. Benjamin/Cummings.